Ultrasonic Acoustic Signal Acquisition and Conditioning Frontend

Comprehensive Design and Simulation Report

Hrishikesh Acharyya

February 2026

Abstract

This report details the theoretical design, mathematical modeling, and SPICE validation of an analog frontend engineered to acquire 45 kHz continuous-wave (CW) tone bursts from an Underwater Locator Beacon (ULB). The architecture implements a piezoelectric hydrophone model, a charge amplifier for signal conversion, an 8th-order Butterworth bandpass filter for rigorous out-of-band noise rejection, and an inverting buffer with a kickback filter for ADC interfacing. Transient and frequency response simulations confirm robust harmonic rejection and a highly linear phase response suitable for downstream Digital Signal Processing (DSP) and Time Difference of Arrival (TDOA) localization. Monte Carlo simulations quantify the worst-case error introduced by component tolerances to ensure manufacturing reliability.

1 Introduction

Acoustic localization of Underwater Locator Beacons (ULB) by Autonomous Underwater Vehicles (AUVs) requires highly resilient analog frontends capable of isolating specific frequency bands while rejecting severe mechanical noise from thrusters, environmental noise, vibrational noise, and electromagnetic interference (EMI) caused by ESC switching. This project presents a complete analog conditioning pipeline bridging a raw piezoelectric hydrophone output to an Analog-to-Digital Converter (ADC).

A ULB-362 beacon from RJE International was chosen as the reference. The beacons transmit an acoustic signal once every second after activation, converting a CMOS-level square wave into a sinusoidal pulse of duration > 9 ms. Detailed specifications can be derived from the device documentation [1].

2 Circuit Architecture

To ensure complete clarity, the entire frontend schematic is divided into three primary functional blocks to process the raw signal from the piezoelectric hydrophone without loss of fidelity.

2.1 Sensor Modeling and Charge Amplifier

Initial system parameters are derived from standard ULB and piezoelectric hydrophone specifications. Given an acoustic output of 160.5 dB re 1μPa at 1 meter [1], the acoustic pressure P in Pascals is:

$$P = 10^{\frac{160.5}{20}} \times 10^{-6} \approx 105.9 \text{ Pa} \tag{1}$$

For the hydrophone, using a worst-case receiving sensitivity of -190 dB re 1V/μPa at 1 meter [2], the voltage sensitivity S_v is:

$$S_v = 10^{\frac{-190}{20}} \approx 3.16 \times 10^{-10} \text{ V}/\mu\text{Pa} \tag{2}$$

Consequently, the estimated unconditioned RMS voltage generated by the sensor at 1 meter is approximately 33.46 mV_{rms}.

To prevent effects of variable cable capacitance, a charge amplifier topology is utilized. The charge amplifier converts accumulated piezoelectric charge directly into a proportional voltage, rendering the system's gain mathematically independent of cable length. The sensor is modeled electrically as a voltage source in series with a capacitance $C_p = 22$ nF and a resistance $R_p = 287$ kΩ as per the topology laid out in [3]. The capacitance and resistance values were calculated by the method shown in [4]

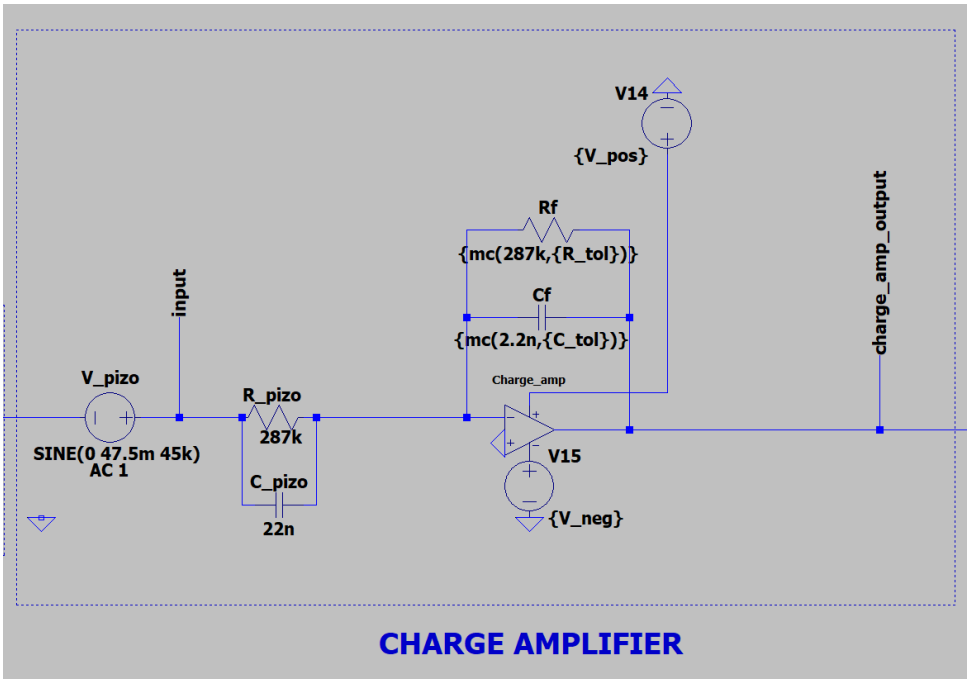

Figure 1: Stage 1: Hydrophone sensor model feeding into the Charge Amplifier.

The generalized transfer function of the inverting charge amplifier is:

$$\frac{V_o}{V_{in}} = -\frac{Z_f}{Z_p} = -\frac{R_f}{R_p}\left(\frac{1 + sR_pC_p}{1 + sR_fC_f}\right) \tag{3}$$

where Z_f is the feedback impedance and Z_p is the source impedance.

From this complete transfer function, the specific passive component values (R_f and C_f) are derived by analyzing the circuit at its frequency extremes:

1. DC Gain ($s \to 0$): At DC, the capacitive reactance approaches infinity, and the transfer function simplifies strictly to the ratio of the resistors:

$$A_{v(DC)} = -\frac{R_f}{R_p} \tag{4}$$

To prevent large DC offsets from saturating the operational amplifier, the DC gain must be restricted. The DC gain is set to unity ($|A_v| = 1$, or 0 dB). Because the hydrophone's internal resistance is $R_p = 287$ kΩ, the feedback resistor is explicitly chosen as $R_f = 287$ kΩ.

2. Midband Gain ($s \to \infty$): At the ultrasonic frequencies of interest, s becomes large, and the sRC terms dominate the numerator and denominator. The transfer function simplifies to the ratio of the capacitances:

$$A_{v(midband)} \approx -\frac{R_f}{R_p}\left(\frac{sR_pC_p}{sR_fC_f}\right) = -\frac{C_p}{C_f} \tag{5}$$

The sensor capacitance was found as $C_p = 22$ nF. To achieve a sufficient initial amplification of 20 dB (a voltage gain of 10 V/V) for the estimated 33.46 mV_{rms} input signal, the feedback capacitor is strategically selected as:

$$C_f = \frac{C_p}{10} = \frac{22 \text{ nF}}{10} = 2.2 \text{ nF} \tag{6}$$

3. High-Pass Cutoff Frequency: The chosen feedback network ($R_f = 287$ k$\Omega, C_f = 2.2$ nF) concurrently establishes the dominant pole of the charge amplifier, forming an intrinsic first-order high-pass filter that effectively rejects low-frequency mechanical drift and vibration:

$$f_c = \frac{1}{2\pi R_f C_f} = \frac{1}{2\pi(287 \text{ k}\Omega)(2.2 \text{ nF})} \approx 252 \text{ Hz} \tag{7}$$

4. High-Frequency Roll-Off and Non-Ideal Behavior: While the ideal transfer function implies infinite bandwidth, the physical charge amplifier will exhibit an intrinsic low-pass roll-off at high frequencies. This behavior is not dictated by the primary feedback network, but rather by the finite Gain-Bandwidth Product (GBW) of the operational amplifier [3].

The high-frequency -3 dB cutoff of the charge amplifier is determined by the intersection of the op-amp's open-loop gain roll-off and the circuit's closed-loop noise gain (A_{noise}):

$$A_{noise} \approx 1 + \frac{C_p}{C_f} = 1 + \frac{22 \text{ nF}}{2.2 \text{ nF}} = 11 \text{ V/V} \tag{8}$$

For an operational amplifier with a specified GBW, the intrinsic low-pass pole occurs at:

$$f_{LPF} \approx \frac{\text{GBW}}{A_{noise}} \tag{9}$$

Assuming a standard high-speed op-amp with a GBW of 100 MHz (as utilized in the SPICE models), the intrinsic low-pass roll-off begins at approximately 9.09 MHz. In the context of the analog frontend, this non-ideal characteristic is highly beneficial, as it acts as a primary, passive anti-aliasing filter that suppresses extreme high-frequency EMI before the signal reaches the active 8th-order Butterworth stages.

3 8th-Order Butterworth Bandpass Filter

To achieve rigorous filtering and to isolate the 45 kHz CW tone, an 8th-order Butterworth bandpass filter was synthesized, establishing a passband from 35 kHz to 58 kHz. The architecture cascades two 2nd-order High-Pass Filters (HPF) [5] and two 2nd-order Low-Pass Filters (LPF) [6] utilizing Multiple Feedback (MFB) topologies [7].

3.1 Computational Synthesis of Filter Parameters

To ensure mathematical rigor, the derivation of the exact component values for the MFB cascaded network was performed using a custom Python computational script. Rather than calculating continuous theoretical values and rounding them—which often leads to severe center-frequency drift in high-Q stages—the algorithm operates by anchoring the math to discrete, commercially available E6 series capacitors.

The algorithm executes the following sequence to bridge the theoretical MFB transfer functions with physical hardware constraints:

1. **E-Series Grid Search:** The script iteratively sweeps through an array of standard E6 series capacitors (100 pF to 10 nF) to use as the foundational variables.
2. **Gain and Topology Constraints:** The script enforces a DC gain of -1 by setting $C_1 = C_3$ in HPF stages and $R_1 = R_3$ in LPF stages
3. **Mathematical Derivation:** For the LPF, the script evaluates the discriminant $(b^2 - 4ac)$ of the MFB design equations, explicitly rejecting capacitor combinations where $C_1 < 8Q^2C_2$ to prevent physically impossible, imaginary resistor solutions. It then solves the quadratic roots to find R_1. For the HPF, algebraic derivations directly yield R_1 and R_2. Equations were derived from [5] and [6]
4. **Practical Boundary Filtering:** The final combinations are rigorously constrained; the algorithm only outputs configurations where the resulting resistors fall within a physically practical and noise-minimized manufacturing range of 1 kΩ to 1 MΩ.

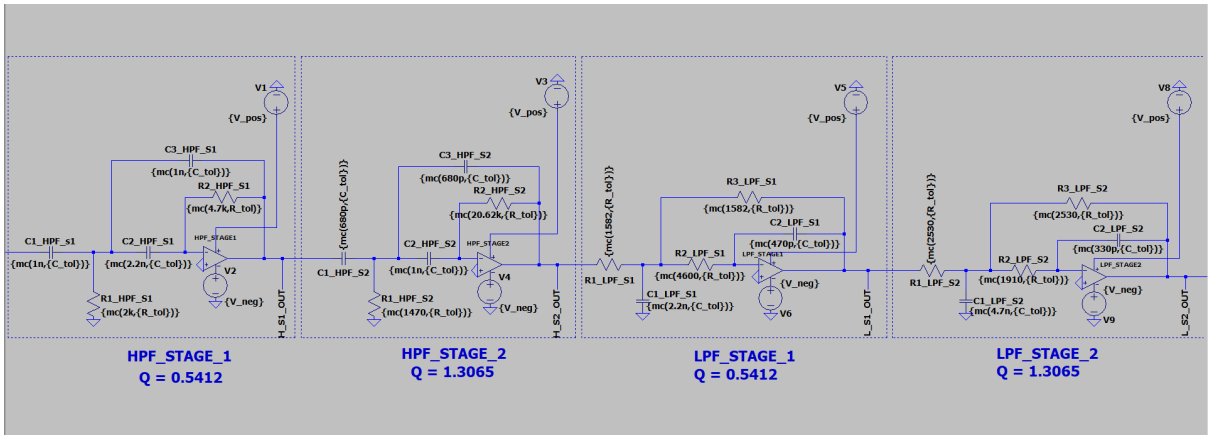

Figure 2: Stage 2: Cascaded HPF and LPF stages forming the 8th-order Butterworth response.

The standard 4th-order Butterworth polynomial dictates stage-specific quality factors of $Q_1 = 0.5412$ and $Q_2 = 1.3065$ [8]. The component values were chosen from the list provided by the script and tweaked according to availability and suitability.

- **High-Pass Filter Stages ($f_c = 35$ kHz):**
  - **Stage 1 ($Q = 0.5412$):** $C_{1,3} = 1$ nF, $C_2 = 2.2$ nF, $R_1 = 2$ kΩ, $R_2 = 4.7$ kΩ.
  - **Stage 2 ($Q = 1.3065$):** $C_{1,3} = 680$ pF, $C_2 = 1$ nF, $R_1 = 1470$ Ω, $R_2 = 20.62$ kΩ.
- **Low-Pass Filter Stages ($f_c = 58$ kHz):**
  - **Stage 1 ($Q = 0.5412$):** $C_1 = 2.2$ nF, $C_2 = 470$ pF, $R_{1,3} = 1582$ Ω, $R_2 = 4.6$ kΩ.
  - **Stage 2 ($Q = 1.3065$):** $C_1 = 4.7$ nF, $C_2 = 330$ pF, $R_{1,3} = 2.35$ kΩ, $R_2 = 1.91$ kΩ.

3.2 Output Stage: Inverting Buffer and Feedthrough Protection

Because the initial charge amplifier stage applies a 180-degree phase shift, an inverting buffer is implemented at the output to restore the signal to be strictly in phase with the incoming acoustic wave. The non-inverting terminal is biased to 1.65 V to perfectly center the AC signal within a unipolar $0 - 3.3$V ADC window.

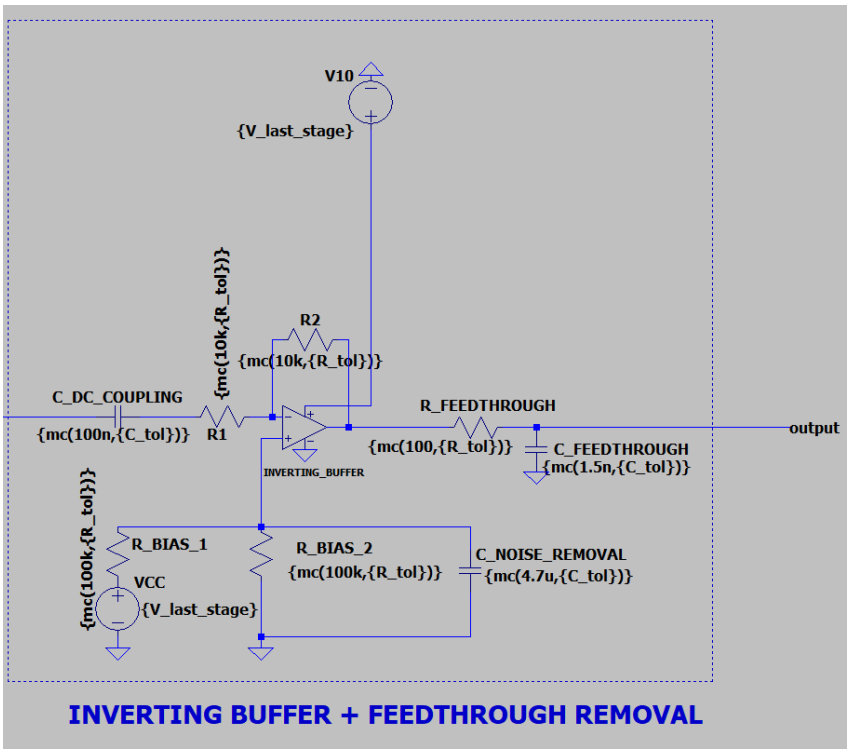

Figure 3: Stage 3: Inverting buffer with DC offset and ADC kickback filter.

To protect against high-frequency ADC sampling transients (kickback) and EMI aliasing into the passband, a passive RC feedthrough filter [9] is implemented at the final output node:

$$f_{alias} = \frac{1}{2\pi R_{ft} C_{ft}} = \frac{1}{2\pi (100\Omega)(1.5\text{ nF})} \approx 1.06\text{ MHz} \tag{10}$$

3.3 Stage 1 Analysis: Charge Amplifier Broadband Response

The initial conditioning stage uses a charge-amplifier topology to convert the high-impedance piezoelectric stimulus into a low-impedance voltage signal. As shown in Figure 4, the stage provides a stable, flat-band gain across the ultrasonic spectrum.

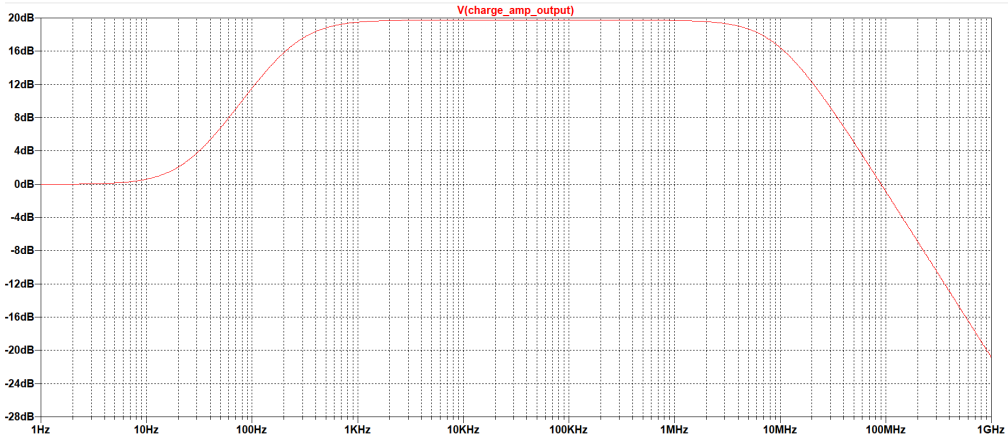

Figure 4: Bode plot of the Charge Amplifier stage (`V(charge_amp_output)`), demonstrating a stable 19.74 dB gain.

The simulated gain of 19.74 dB aligns with the theoretical target of 20 dB ($C_p/C_f = 10$), with a negligible 1.28% variance attributed to tolerance error.

Table 1: Charge Amplifier Simulation Results

Parameter	**Theoretical**	**Simulated**	**—%Error—**
Midband Gain	20.00 dB	19.744 dB	1.28%
Upper 3dB cutoff	9.09 MHz	9.33 MHz	2.46%
Lower 3dB cutoff	252.06 Hz	242.84 Hz	3.65%

3.4 Overall System Response: 8th-Order MFB Filter

The complete signal chain incorporates a cascaded 8th-order Butterworth filter to isolate the target 45 kHz CW beacon. Figure 5 illustrates the total system response, characterized by steep roll-off rates exceeding -80 dB/decade in the stopbands.

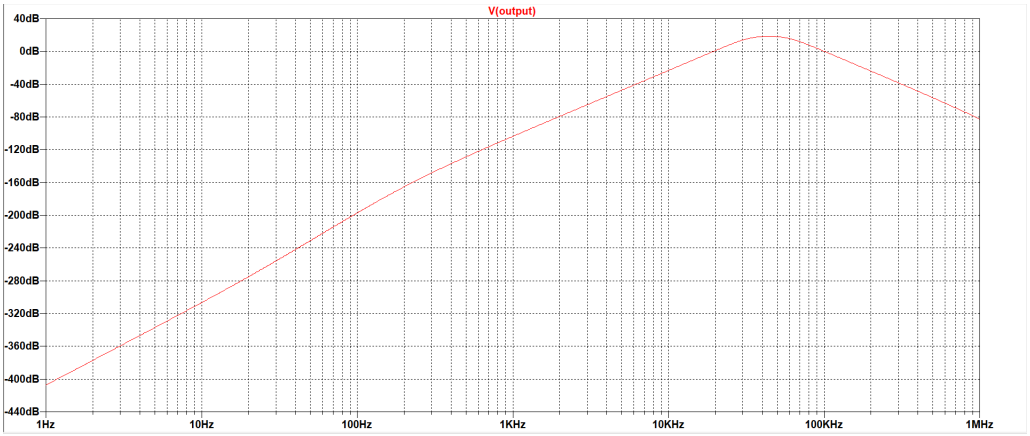

Figure 5: Overall system frequency response (`V(output)`) showing the 35–58 kHz passband.

The measurement of the system-wide gain at 18.45 dB is accounted by component tolerance errors. The -3 dB cutoff frequencies were programmatically extracted to confirm passband compliance.

Table 2: Integrated System AC Parameters

Parameter	**Target**	**Simulated**	**% Error**
Peak System Gain	20.00 dB	18.45 dB	7.75 %
Lower Cutoff (f_L)	35.00 kHz	32.06 kHz	8.4%
Upper Cutoff (f_H)	58.00 kHz	60.24 kHz	+3.86%
-3 dB Bandwidth	23.00 kHz	28.18 kHz	+22.5%

3.5 Steady State Transient Analysis and Phase Integrity

Transient simulations confirm the phase inversion of the charge amplifier (Figure 6) and the successful rectification by the final buffer stage (Figure 7). The output waveform is strictly in phase and sits perfectly on the 1.65 V DC bias. The measured output amplitude of 788.7 mVp-p reflects a minor, expected attenuation from the theoretical 950 mV due to cumulative passive component tolerances (Figure 8).

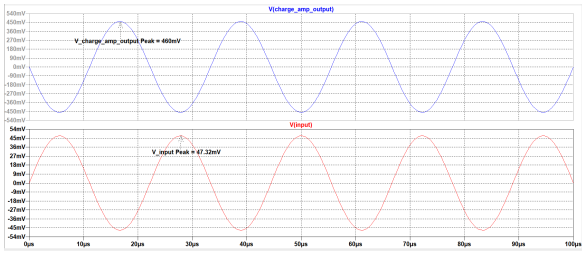

Figure 6: Charge amp output exhibiting theoretical 180° phase inversion.

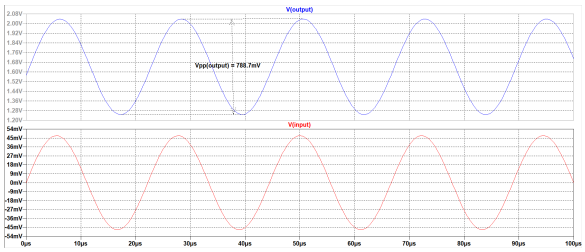

Figure 7: Final conditioned output: In-phase and DC-shifted to 1.65 V.

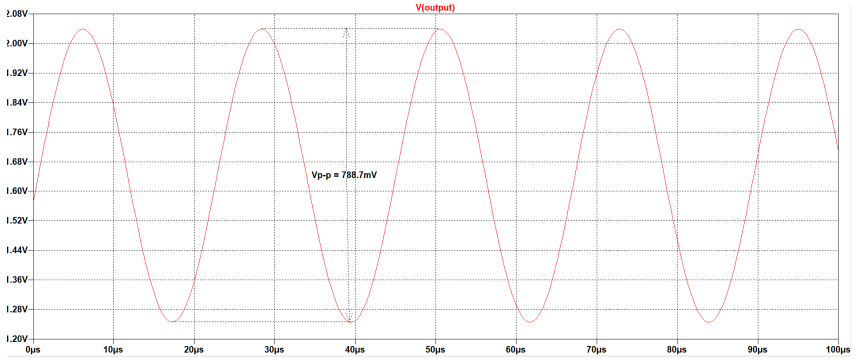

Figure 8: Amplitude measurement of 788.7 mVp-p.

3.6 Harmonic Rejection

To rigorously test the 8th-order roll-off, severe harmonics at 90 kHz and 135 kHz were injected into the input stimulus. As illustrated in Figure 9, the system aggressively strips the out-of-band interference, yielding a pristine fundamental tone ready for thresholding.

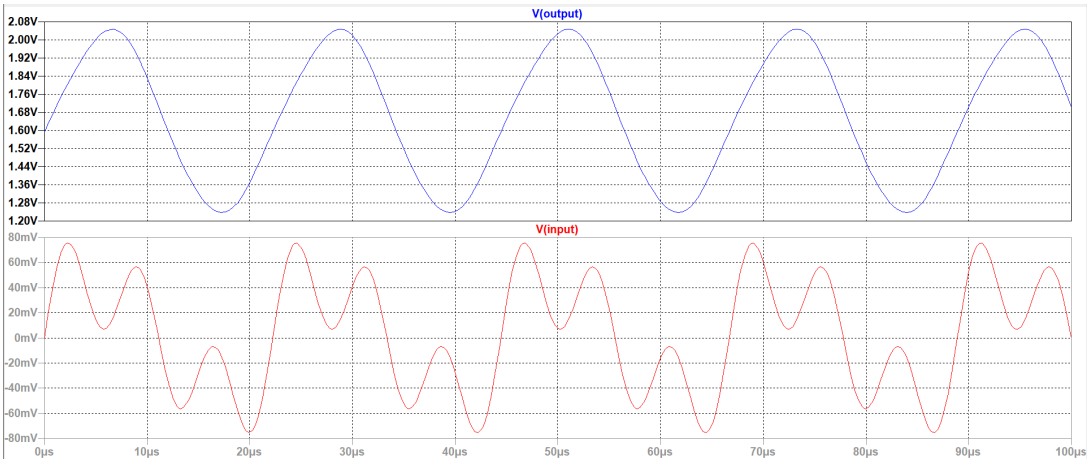

Figure 9: Robust harmonic rejection: Polluted input (bottom) vs. Filtered output (top).

3.7 Monte Carlo Simulation

To understand the effect of component tolerances on the viability of the frontend for Time difference of arrival work and to quanitfy the worst case channel to channel error introduced a Monte Carlo simulation was run and Figure 10 was obtained

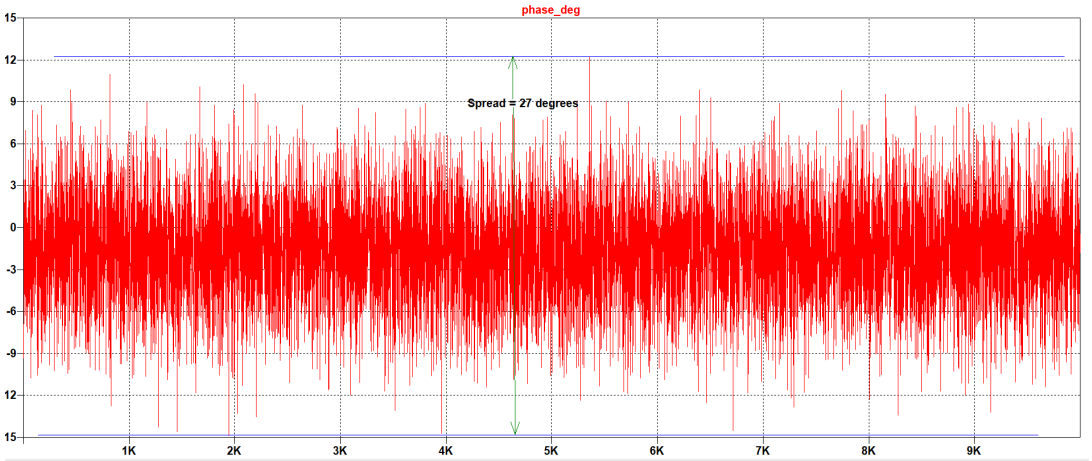

Figure 10: Iterations vs phase angle at 45khz. The spread is 27 degrees.

4 Conclusion

The analog frontend successfully conditions 45 kHz acoustic signals while providing rigorous harmonic rejection and unwanted noise removal. Monte Carlo analysis confirmed a worst-case phase drift of 27° between channels, which is not detrimental for short-range passive acoustic localization

4.1 Future Work

- **Group Delay Optimization:** Address the observed 9μs group delay to enhance real-time TDOA performance. This can be done by using Bessel-Butterworth hybrid filters
- **Dynamic Gain Control:** Integrate a Programmable Gain Amplifier (PGA) to maintain signal integrity as beacon distance varies.
- **Hardware Prototyping:** Transition from SPICE validation to PCB fabrication to assess real-world SNR.
- **Component selection:** Select components with lesser tolerances or use Leapfrog filters or other such topologies to reduce the effect of component tolerances

5 Complete System Schematic

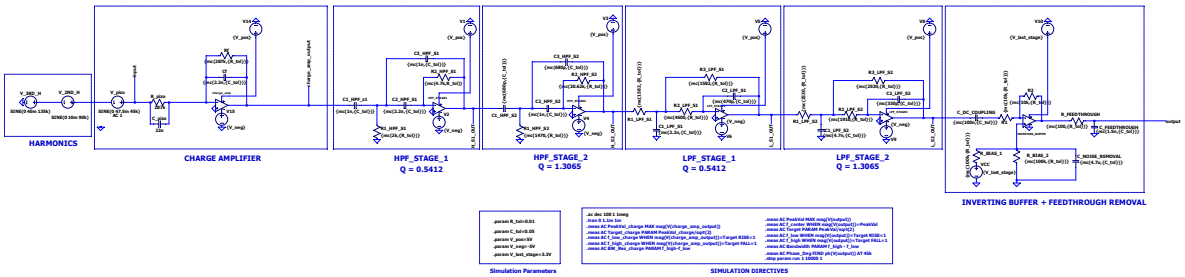

--- E:\acoustics\ADC_frontend_filter\adc_frontend.asc ---

Figure 11: Complete System Schematic: Charge Amplifier, 8th-Order Filter, and Output Buffer.

References

[1] RJE International, Inc., *ULB-362 Series Underwater Locator Beacon User's Manual*, May 2015.

[2] Aquarian Audio Products, *H1c Hydrophone User's Guide*.

[3] J. Karki, "Signal conditioning piezoelectric sensors," Application Report SLOA033A, Texas Instruments, September 2000.

[4] A. Shaw, A. Kumari, H. P. S. Kumar, S. K. Kar, A. Dutta, and S. Kundu, "Design considerations of signal acquisition circuit development for piezoelectric pressure sensor," in *2024 IEEE 21st India Council International Conference (INDICON)*, pp. 1–5, IEEE, 2024.

[5] "Single-supply, 2nd-order, multiple feedback high-pass filter circuit," analog engineer's circuit cookbook: amplifiers, Texas Instruments, 2022.

[6] "Single-supply, 2nd-order, multiple feedback low-pass filter circuit," analog engineer's circuit cookbook: amplifiers, Texas Instruments, 2022.

[7] M. Steffes, "Design methodology for mfb filters in adc interface," Application Report SBOA114, Texas Instruments, February 2006.

[8] M. E. Van Valkenburg, *Analog Filter Design*. New York: Oxford University Press, 1982.

[9] J. Karki, "Active low-pass filter design," application note, Texas Instruments, 2023.